

Manufacturing cosmic rays in the evolving dynamical states of galaxy clusters

Reju Sam John ^{1,2}, Surajit Paul ^{2,3} ^{*}, Luigi Iapichino ⁴, Karl Mannheim ⁵
and Harish Kumar ¹

¹ Department of Physics, Pondicherry Engineering College, Puducherry, 605014, India

² Department of Physics, SP Pune University, Pune, 411007, India

³ Inter-University Centre for Astronomy and Astrophysics, Pune, 411007, India

⁴ Leibniz-Rechenzentrum der Bayerischen Akademie der Wissenschaften, Boltzmannstr. 1, D-85748 Garching b. Munchen, Germany

⁵ Lehrstuhl für Astronomie, Institut für Theoretische Physik und Astrophysik, Universität Würzburg, Emil Fischer-Str. 31, D-97074 Würzburg, Germany

Accepted . Received ; in original form

ABSTRACT

Galaxy clusters are known to be the reservoirs of Cosmic Rays (CRs), mostly inferred from theoretical calculations or detection of CR derived observables. Though CR electrons have been detected through radio emissions, CR protons and its derivative gamma rays remained undetected. CR acceleration in clusters is mostly attributed to its dynamical activities that produce shocks. Shocks in clusters emerge out of merger or accretion but, which one is more effective? at which dynamical phase? and why? So, in quest of answers, we study the detail evolution of cosmic ray emission in the galaxy clusters using cosmological simulations with ENZO code. Defining appropriate dynamical states using the concept of virialization, we have studied a sample of merging and non-merging clusters. We report that the merger shocks (Mach, $\mathcal{M} = 2 - 5$) are the most effective CR producers in clusters. Clusters once merged, permanently deviate from CR and X-ray mass scaling of non-merging systems, enabling us to use it as a tool to determine the state of merger. Through a temporal and spatial evolution study, we found a strong correlation between cluster merger dynamics and CR production. We have observed that the brightest phase of X-ray and CR emission from clusters occur respectively about 1.0 and 1.5 Gyr after every merger. This significant finding of non concurrent appearance of X-ray and CR emission peaks can explain the non-detection of gamma-rays from many X-ray bright galaxy clusters. This can also be a guiding information to select appropriate targets for gamma-ray detection from clusters.

Key words: galaxies: clusters: cosmic ray: clusters mergers - dynamical states - hydrodynamics - methods: numerical

1 INTRODUCTION

Being on the top of the large-scale structure mass hierarchy, galaxy clusters, during its emergence and Giga years (Gyr) of evolution time, witness a cascade of dynamical events. Studies have confirmed that the galaxy clusters had emerged out of the aggregation of structures like galaxies, groups of galaxies, hot inter-cluster medium and warm hot materials from the filaments (Bykov et al. 2015; Yu et al. 2015; Springel et al. 2006). The energy budget of galaxy clusters are thus the cumulative effect of all possible dy-

namical events such as star formation, supernova activity, AGN activity, galaxy formation and structure mergers at all levels (galaxy, groups, clusters). Recently, a possible role of Dark Matter (DM) annihilation has been claimed (Planck Collaboration et al. 2013; Huber et al. 2013; Berezhinsky et al. 1997). So, galaxy clusters are among the best available cosmic laboratories (Blasi 2004; Berezhinsky et al. 1997; Huber et al. 2013) to test the energy evolution of the universe. Though a major fraction of the energy in the clusters is thermal in nature, a non-negligible non-thermal component is also present (Brunetti & Jones 2014; Petrosian & Bykov 2008). The main contributors to the non-thermal energy component are gamma rays, secondary gamma rays,

* E-mail: surajit@physics.unipune.ac.in

non-thermal hard X-rays, radio waves (Brunetti & Jones 2014; Kushnir & Waxman 2009). The claims of observation of hard X-ray (Nevalainen et al. 2004; Kushnir & Waxman 2010) and gamma emission (Xi et al. 2017) from galaxy clusters can be interpreted as direct evidence for the existence of such non-thermal component. On the other hand, Mpc scale radio sources observed in the cluster centre or at the outskirts are the indirect but strong evidence of presence of non-thermal i.e., Cosmic Ray (CR) particles and magnetic fields (for review: Kaastra et al. (2008)).

Galaxy clusters usually grow by continuous accretion and mergers of smaller and bigger groups of galaxies. Mergers of galaxy clusters in the mass range between $10^{14} M_{\odot}$ and $10^{15} M_{\odot}$ release an enormous binding energy of about 10^{63} to 10^{65} ergs. It has been proposed that the energy released during these mergers creates huge pressure in the cluster core (Paul 2012). As a result, the medium starts expanding supersonically inducing strong shocks in the baryonic gas (Kang et al. 1996; Miniati 2000; Paul et al. 2011; Kang & Ryu 2013). Merger energy then gets dissipated mainly through shock heating and turbulence stirring in the medium (Sarazin & White 1987; Dolag et al. 2005; Iapichino et al. 2010; Bourdin et al. 2013). Moreover, due to shock acceleration, a significant amount of charged particles gains energy and reaches the non-thermal regime by converting the shock energy and thus contributing to the CR population (Berrington & Dermer 2003; Sarazin 2001; Jones et al. 2001). As energy gets dissipated, clusters tend to attain a state of virialisation. At the point of virialisation, almost an equipartition of gravitational energy to kinetic energy can be observed. Roughly a thermodynamic equilibrium is also expected to be established in the cluster medium, if a sufficiently long time is elapsed before it reaches the virialisation (Ballesteros-Paredes 2006). Clusters deviating from this equilibrium are either having more potential energy (usually this is the phase of a rapid mass accretion/merger) or having more kinetic energy in the course of relaxation (i.e. a state of disturbance or higher entropy) (Barsanti et al. 2016).

Usually shocks due to mergers emerge at the central core of the newly formed clusters and travels radially as spheroidal wave-front towards the virial radius and beyond (Paul et al. 2011; Iapichino et al. 2017; van Weeren et al. 2011; Paul 2012; Bagchi et al. 2006, 2011). Time-scale of such dissipation for a single merger is found to be about 1-2 Gyr (Paul et al. 2011; Roettiger et al. 1999) indicating an energy dissipation rate of the order of $10^{47} \text{ erg s}^{-1}$. In this process, the thermal particles in the medium are injected at the shocks and a fraction of them gets accelerated to high energy CR particles through collision-less shock-energy-dissipation (Malkov 1998; Ellison & Ramaty 1985). Also, pre-existing high-energy particles originated from other processes such as numerous star-formation events, supernovae explosions, AGN activity etc., can further be accelerated to very high energies through multiple shock crossings (Kang & Jones 2007). So, it is quite evident that a fraction of these particles from the thermal pool gets converted into non-thermal CRs, mainly via diffusive shock acceleration (DSA Blandford & Eichler 1987, Malkov & O’C Drury 2001). The cosmic ray production due to shock acceleration is then expected to be more prominent during the post merger violent relaxation phase. This indicates a possible strong connection of

CR emission and the dynamical state of the cluster systems (Brunetti & Jones 2014).

Compared to CR electrons, CR protons have larger radiative cooling time, quantitatively by the square of the mass ratio, $(m_p/m_e)^2$ and are estimated to be of the order of 3-30 Gyr. Having such a high cooling time, protons accelerated by accretion shocks at the outskirts of the cluster can accumulate in the galaxy clusters spanning the Hubble time (Hong et al. 2014; Völk et al. 1996). So, clusters are expected to be major source of high energy CRs. But, surprisingly, no firm detection of gamma rays from clusters are reported yet. The reasons for this non-detection has not been addressed or explored well yet. However, the non detection of gamma-ray emission from galaxy clusters (for the most recent data, see Ackermann et al. 2016) puts constraints on the content of CR protons in the cluster centres (Brunetti et al. 2017 and references therein).

In this paper, we study the emission and evolution of CR particles in the merging and non-merging galaxy clusters to understand the brightest phase CR emissions from clusters. Specifically, we try to understand what are the main factors that control the CR emission in clusters, in terms of the link between dynamical states of clusters to their energy distribution, and to observable diagnostics like the X-ray luminosity. We use the concept of virialisation (see section 3.1.2) and merger energy distribution (see section 5.1) to characterise the dynamical state of the simulated galaxy clusters. The simulations, run with the ENZO code (Bryan et al. 2014) includes the effects of star formation, supernova (SN) feedback and cooling due to radiative processes. For our cosmological simulations of structure formation, AGN feedback has not been considered as it is unlikely to have any significant impact on scales of high-mass objects like galaxy clusters (Le Brun et al. 2014; McCarthy et al. 2010). Also, the only mechanism considered for CR acceleration in this work is the first-order Fermi process with pre-existing CRs from AGN and supernova, neglecting therefore the second-order Fermi acceleration and explicit contribution from SNs and AGNs.

Our paper is organised as follows. After giving the introduction in section 1, we will start with the description of our simulations, simulated realisations in Section 2. Sample selection will be made in Section 3. Modelling useful thermal and non-thermal energies for this work has been described in the section 4 and evolution of dynamical parameters has been explained in Section 5. In Section 6, we have reported findings and discussed the results. Linking energetics of clusters with merging events and to the dynamical states will also be reported in this section. A brief discussion on the limitations of this work has been written in section 7. Finally, we will summarise the outcome in section 8.

2 SIMULATIONS OF CLUSTER MERGERS AND ITS ANALYSIS DETAILS

To create a sample of galaxy clusters, simulations were performed with the Adaptive Mesh Refinement (AMR), grid-based hybrid (N-body plus hydrodynamical) code ENZO v. 2.2 (O’Shea et al. 2005; Bryan et al. 2014). This code uses adaptive refinement in space and time, and introduce non-adaptive refinement in mass by multiple child grid insertions. A flat Λ -CDM background cosmology with specific

cosmology parameters $\Omega_\Lambda = 0.7257$, $\Omega_m = 0.2743$, $\Omega_b = 0.0458$, $h = 0.702$ and primordial power spectrum normalisation $\sigma_8 = 0.812$ has been used. Cosmology parameters are obtained from Λ -CDM cosmology, derived from WMAP (5-years data) combined with the distance measurements from the Type Ia supernovae (SN) and the Baryon Acoustic Oscillations (BAO) (see Komatsu et al. (2009)). Simulations have been initialised at redshift $z = 60$ using the Eisenstein & Hu (1999) transfer function, and evolved up to $z = 0$. An ideal equation of state was used for the gas, with $\gamma = 5/3$.

Our research mainly focuses on the production of CRs through Diffusive Shock Acceleration (DSA), which is a strong function of shock strength. Detection and quantification of shocks is thus an important part of this project. Merger shocks compress the medium near to the shock front, but post shock medium suffers rapid expansion and can induce radiative cooling (Akahori & Yoshikawa 2012; Choi et al. 2004). We have thus used the cooling and heating model of Sarazin & White (1987) that takes into account the effect of radiative cooling due to X-ray emissions and heating due to star formation, star motions and SN. Further, we have used the star formation and feedback schemes of Cen & Ostriker (1992) with a feedback of 0.25 solar. We have named this model with additional physics as ‘coolSF’ runs (for details, see Paul et al. (2017)). Shocks have been detected in our simulations using un-split velocity jump method of Skillman et al. (2008) with a temperature floor of 10^4 K which is found to give better results in AMR simulations (Vazza et al. 2011).

Since shocks are a vital component of our study, in our adaptive mesh refinement strategy, we have used the refinement criteria based on shocks along with the over-density. Over-density criteria has been used on both the DM and the baryon component. The cells will be flagged for refinement if the local density ρ_i , where ‘i’ can indicate either baryons or DM, fulfils the following criterion:

$$\rho_i > f_i \rho_0 \Omega_i N^l \quad (1)$$

where $\rho_0 = 3H_0^2/8\pi G$ is the critical density, H_0 is the Hubble parameter at the present epoch, Ω_i are the cosmological density parameters for either baryons or DM, and the refinement factor is $N = 2$. Here l is the refinement level (for root grid, $l = 0$). In the current work we set $f_i = 4$ for both the overdensities $f_b = f_{DM} = 4$. Since density is very low on the outskirts of the large-scale objects compared to their innermost parts, the AMR based on overdensity is not suitable for refining the flow there (Iapichino et al. 2017). For this reason we also require an additional AMR criterion, whose effectiveness does not depend strongly on density. We use therefore the refinement on shocks as additional AMR criterion. The Mach number of a shock is not a direct function of density, but it depends on the ratio of post and pre-shock densities. This is the reason why, even at regions far away from the centre, where density is very low, we could still reach up to the highest level of refinement at the shocked regions. Enstrophy, derived from vorticity field has been earlier used by Iapichino et al. (2017) for similar purposes.

We have first produced several low-resolution, dm-only runs to select suitable clusters depending on their mass, size and dynamical history and re-simulated them at high resolutions with the full physics setup. The evolution and mass accretion of the forming structures have been followed by

producing merger trees with the yt toolkit (Turk et al. 2011). Our main simulations are of $(128 \text{ Mpc h}^{-1})^3$ volume and utilise a root grid with 64^3 elements. We have introduced 2 nested child grids. Furthermore, 4 additional AMR levels are used in the central $(32 \text{ Mpc})^3$ volume. The effective spatial resolution is thus of about 30 kpc for the simulations of our reference set (‘RefRES’ hereafter). We have performed a resolution study using some lower and higher resolution and different root grid resolution simulations compared to our RefRES. For a detailed resolution study please refer Appendix A.

3 SAMPLE SELECTION

For this study, we have simulated ten galaxy clusters with ‘CoolSF’ physics (Section 2). From five different realisations of the low-resolution, dm-only setup, we have chosen the objects that in our judgement seemed to be better representative of different mass ranges and dynamical states. The cluster mass in our samples varies from a lowest of $10^{13} M_\odot$ to the highest of $> 10^{15} M_\odot$, providing almost two orders of magnitude in mass to study a wide range of systems (for details of these simulated clusters see Table 1).

For identifying objects in our simulations, we have used virial radius as a delimiter, where, ‘virial’ refers to the quantity at over density of 200 to the critical density of the universe at that redshift. In the further text, over density should be understood as compared to the critical density only. Though, we have focused on a central cluster in each high-resolution run, a large number of smaller objects are available within the $(32 \text{ Mpc})^3$ central volume of our simulations where AMR has been allowed. So, along with the main 10 clusters, for statistical studies, we have a few hundred clusters with the same resolution by combining the data from different sets of simulations. The number has further been increased by considering the output snapshots from various redshifts. We made sure that the DM particles and baryon gas that forms the objects of interest are mostly coming from the well refined Lagrangian region. To do so, we have taken the objects that are placed only within central $(20 \text{ Mpc})^3$ volume. Though in our simulations, we have galaxy groups with mass about $10^{13} M_\odot$, it has been observed that low mass systems does not follow the cluster mass scaling (Bharadwaj et al. 2015; Paul et al. 2015, 2017). So, to ensure roughly the cluster properties of these systems as well as enough statistics and mass range, the minimum mass we have considered for our study is $5 \times 10^{13} M_\odot$. We did not put any cut-off on highest mass and our list contains mass upto $2 \times 10^{15} M_\odot$. Mass resolution at the innermost child grid in our simulations is less than $10^9 M_\odot$ i.e. with more than 10^4 particles provide enough resolution for even the smallest objects used. Also, with 30 kpc effective resolution, systems above $5 \times 10^{13} M_\odot$ having r_{200} above 500 kpc, get adequately resolved in space.

3.1 Sampling by dynamical activities

3.1.1 Merging and non-merging systems

In our high resolution simulation sample of 10 clusters (Cl₁ to Cl₁₀ in Table 1), we have chosen 6 merging systems and

Table 1. Cl_1 to Cl_{10} are the highly refined clusters in our simulation samples. Total mass and the baryonic mass of the listed clusters are given in the 2nd and 3rd column respectively. These are the masses within the radius R_{200} or virial radius and radius R_{500} , which is given in the 4th column. Similarly, temperatures are given in the 5th column. Finally, the merging state of each of these clusters is reported in the 6th column.

Run	Virial Mass (T) ($10^{14} M_{\odot}$) R_{200}/R_{500}	Virial Mass (B) ($10^{14} M_{\odot}$) R_{200}/R_{500}	Virial Radius (Mpc) R_{200}/R_{500}	Virial Temperature ($10^7 K$) R_{200}/R_{500}	Merging State
Cl_1	24.81/21.03	3.62/3.05	3.70/2.76	4.73/6.21	Non-merging
Cl_2	15.67/12.58	2.23/1.76	3.17/2.27	4.13/5.05	Merging
Cl_3	9.08/7.78	1.34/1.12	2.64/1.96	2.87/3.74	Merging
Cl_4	9.41 /7.57	1.29/1.05	2.74/1.97	2.58/3.06	Merging
Cl_5	9.41/7.33	1.31/1.04	2.70/1.97	2.70/3.41	Non-merging
Cl_6	7.26/6.67	0.96/0.86	2.57/1.83	2.46/3.91	Merging
Cl_7	6.99/5.77	0.97/0.81	2.42/1.80	2.24/2.82	Merging
Cl_8	6.72/5.55	0.94/0.75	2.47/1.74	1.84/2.73	Non-merging
Cl_9	0.89/0.78	0.11/0.09	1.21/0.91	0.59/0.73	Merging
Cl_{10}	0.88/0.72	0.12/0.10	1.23/0.88	0.58/0.82	Non-merging

4 non-merging systems. We have computed the merger trees for these objects and accordingly indicated the merging and non-merging systems. A non-merging, relaxed galaxy cluster is a system that has not experienced any merger with a mass ratio larger than 0.1 almost for the last 8 Gyr (from redshift $z = 1.0$ to the current epoch ($z = 0$)). i.e. almost all its evolution time (e.g. see the column 6 in Table 1). All other systems are labelled as mergers. Merging systems are spanning from small mergers (ratio more than 0.1 but less than 0.3) to major mergers (ratio more than 0.3, for definition see: Paul et al. (2011) and references therein). Also, there is a cluster that got merged only once (e.g. Cl_7) and a system with multiple mergers (e.g. Cl_2). We have chosen the biggest two i.e. Cl_1 (non-merging) and Cl_2 (merging) as the primary representative of non-merging and merging samples as their final mass is almost identical (about $2 \times 10^{15} M_{\odot}$) and they truly represent their class. The masses of all other clusters in the list are chosen very carefully to compare them well. Each of the non-merging systems has at least one comparable merging system with similar mass. These clusters are mainly used to study the time evolutions of different physical parameters. We have used different pairs of systems for comparing different parameters depending upon requirements (e.g. mass range, number of mergers etc.).

3.1.2 Dynamical states of galaxy clusters using the concept of virialisation

Evolving galaxy clusters are dynamically very active and cannot attain virial equilibrium in a time shorter than their dynamical time-scale (Ballesteros-Paredes 2006). For a self gravitating system like the clusters, the corrected form of virial theorem can be expressed as below (Davis et al. 2011).

$$\frac{1}{2} \frac{d^2 I}{dt^2} = 2K + W - E_s \quad (2)$$

Where, I is the moment of inertia of the system and K and W represent the kinetic energy and gravitational potential energy of the system respectively. For the systems like the galaxy clusters where, influence of external potential (i.e. out side the virialised radius) is significant, W can

be expressed as $U_{int} + U_{ext}$, where U_{int} is the internal potential of the studied system and U_{ext} is due to the mass outside the cluster radius (here, r_{200}) but, whose tidal effect can be felt. The surface pressure term E_s comes from the velocity dispersion of the galaxies that creates an extra outwards force on the cluster virial surface. At the time when the double derivative of I vanishes, the system said to have attained the virial equilibrium (Ballesteros-Paredes 2006; Davis et al. 2011).

To study the virialisation of galaxy clusters, we have defined virial ratio as

$$\mathcal{R}_1 = \frac{(U_{int} + U_{ext} - E_s)}{2 * KE} \quad (3)$$

The ratio should be unity for a perfect virialised system. We have plotted the evolution of this ratio for pairs of clusters of similar mass but different dynamical state, namely (Cl_4 and Cl_5) and (Cl_9 and Cl_{10}) in Figure 1. Here, we have also shown single (Cl_4) and multiple (Cl_9) merging systems. From a comparison of the two panels of Figure 1 one can clearly see that, during mergers (visible as a steep mass increase in Fig. 1(b)), the virial ratio has boosts (Fig. 1(a)) too, because the system gains potential energy very fast and also dissipates to various other energy forms in about a Gyr time. In contrast to merger, non-merging systems (i.e. Cl_5 and Cl_{10}) mostly remained virialised for the whole life span. Fig 1, clearly shows that a moderate change in the mass is hugely reflected in virial ratio (\mathcal{R}_1), making it clearly identifiable. From a qualitative analysis of Figure 1(a) one can see that, for merging clusters, about one third of the life span remain out of virialisation.

The systems with \mathcal{R}_1 values much larger or smaller than 1 are respectively either out of steady state or are thermally agitated. So, the dynamical state of any system can be determined very accurately, if we know how far a system is from $\mathcal{R}_1 = 1$. So, it would be interesting to characterise the dynamical state of the clusters in our sample, in terms of the virialisation parameter defined in Equation 3.

We have chosen about 384 galaxy clusters from different snapshots of our ten realisations. Chosen clusters are in the mass range (virial mass at r_{200}) of $5 \times 10^{13} M_{\odot}$ to $2 \times 10^{15} M_{\odot}$ in between redshift $z = 0.5$ to $z = 0$. Our

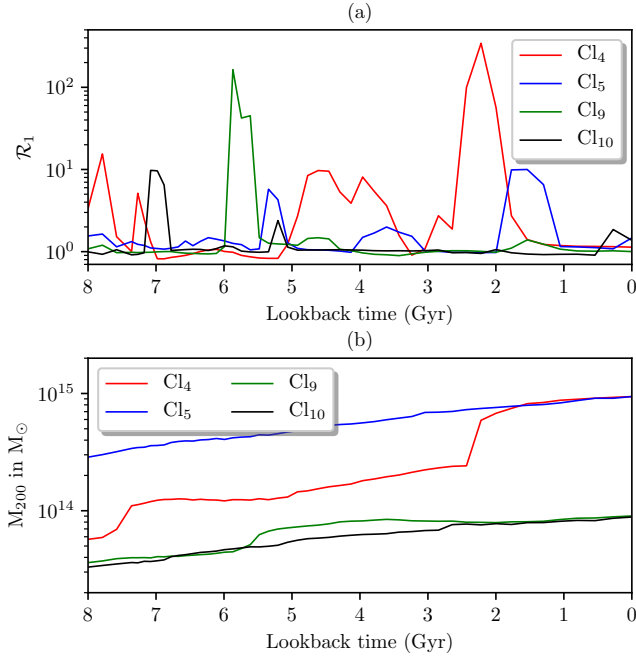


Figure 1. Panel (a): Time evolution of virial ratio (\mathcal{R}_1) of merging and non-merging clusters. Panel (b): Mass evolution of the same clusters.

simulations though show a statistical mean of this ratio at about 1.00 (more precisely 0.996) considering a Lorentzian distribution to accommodate the slight asymmetry in the distribution (see Fig 2). For the same systems, if we compute the ratio $\mathcal{R}_2 = \text{PE}/2\text{KE}$, the statistical mean comes at 1.23 (Fig 2, dotted line), more than 20% away from $\mathcal{R}_1 = 1$. This deviation is known to occur if the surface pressure term arising due to the kinetic stresses at the surface of the collapsing clouds and the external potential due to mass outside the virial radius are not considered for calculating virial ratio (Ballesteros-Paredes 2006; Shaw et al. 2006).

Wen & Han (2013) found that, in their sample, there are 28% of relaxed clusters. Motivated by analogy with observations, we see that in our sample has about the same fraction of clusters within 10% from 1.0. Thus we define these objects as “virialised”. The clusters that are either having low virial ratio or high ratio will be called as non-virialised clusters in our paper. We have found 278 objects i.e. about 2/3 of the all considered galaxy clusters as non-virialised. A high number of non virialised objects could have been resulted due to inclusion of low mass systems (i.e. less than $10^{14} M_\odot$) as smaller clusters are expected to be unstable to dynamical activity or mostly non-virialised (Diaferio et al. 1993; Paul et al. 2015, 2017). Non-virialised objects are further divided in to two categories, namely, ‘HighPE’ i.e. objects with higher potential energy (i.e. PE greater than 2KE) and the objects with higher kinetic energy as ‘HighKE’ (i.e. 2KE greater than PE).

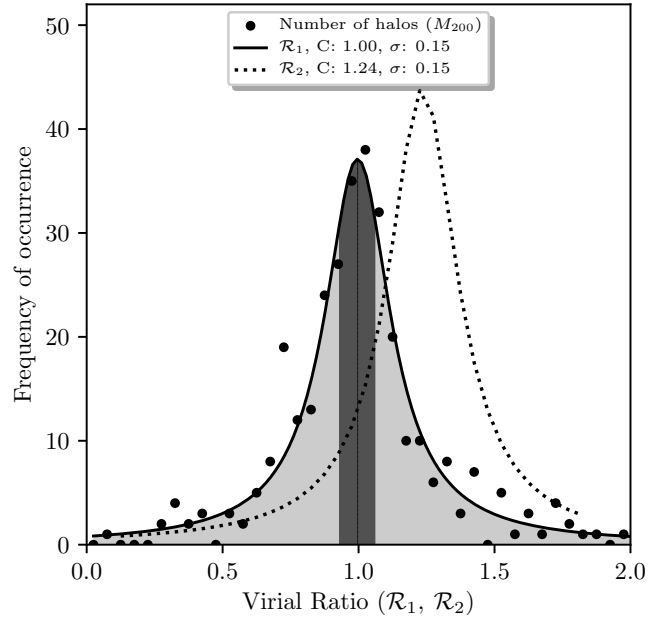


Figure 2. Virial ratio \mathcal{R}_1 of the galaxy cluster samples are plotted (solid line) according to their frequency of occurrence within bins of size 0.05 in a span of 0-2. A Lorentzian is fitted to this frequency plot to compute the statistical mean and the dispersion. Occurrence of ratio \mathcal{R}_2 has been plotted and fitted as earlier with dotted line.

3.2 Cluster scaling test of the samples

After categorising our sample, we have computed the virial mass (total) and temperature for all the virialised clusters. Assuming that for virialised clusters the assumption of hydrostatic equilibrium holds, we aim to check to which extent the well-known scaling relations are valid for them. Self similar relations between the mass, temperature and the virial radius of cluster are given by $M_{vir} \propto r_{vir}^3$ and $T_{vir} \propto M_{vir}/r_{vir}$ i.e. $T \propto r_{vir}^2$ and $T \propto M^{2/3}$ (e.g., Peebles (1980); Kaiser (1986)). However, observation does not favour this, rather it shows a steeper slope (Maughan et al. 2012). Pre-heating of ICM, non-uniform shock heating, loss of energy to star-formation, non-thermal emissions and so on. i.e. all non-hydrostatic parameters are the major reason for deviation from self similarity (Finoguenov et al. 2001; Nevalainen et al. 2000; Ponman et al. 1999). Also, as these are connected to the dynamical activity of the clusters, they are the prime reasons for many clusters being non-virialised (Aguirri & Sánchez-Janssen 2010). Our ‘CoolSF’ model has been tested and observed to corroborate very well with observations when complete data set for galaxy clusters are considered (Paul et al. 2017). Since deviation from cluster scaling are mainly attributed to dynamical activities, we expect to find the M-T relation to be close to the theoretical value for perfectly virialised objects, but total sample should show a value close to observed value.

A simple check would help us to validate our choice of virialised objects by testing its M-T relation. To do so, we have plotted these parameters and fitted scaling laws

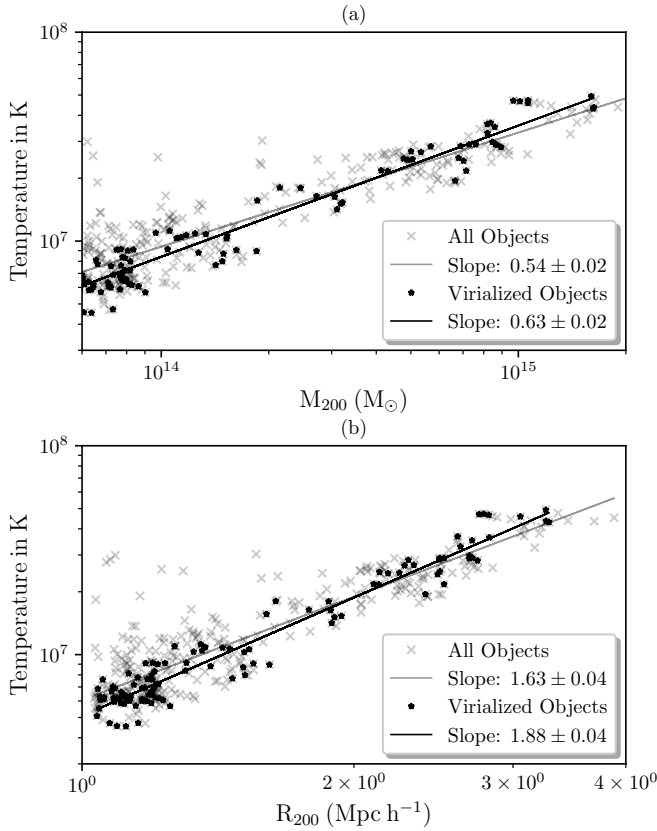


Figure 3. Panel (a): Total mass of the virialised fraction of our sample is plotted against the temperature of the respective clusters. Panel (b): virial radius is plotted against the temperature of the systems.

(see figure 3). The statistical fit of the parameters of the chosen virialised clusters in our simulations (Fig 3, black dots and fitted line) shown to obey almost the expected theoretical value of $T \propto r_{vir}^2$ and $T \propto M_{vir}^{2/3}$. The scattered points found in the plots are indicating slight deviation from the exact virial condition. Whereas, when we take all the objects from our sample list (Fig 3, all points and grey fitted line), it closely matches with the observational values of $T \propto M^{0.55}$ and $T \propto r_{vir}^{1.7}$ (Finoguenov et al. 2001; Shimizu et al. 2003; Arnaud et al. 2005; Vikhlinin et al. 1999). For all other parameters such as L_X -T, L_X -M etc., please check Paul et al. (2017).

4 MODELLING X-RAY AND COSMIC RAY EMISSIONS

4.1 Thermal X-ray emissions

Merger induced shocks, gas drag by the density clumps and other similar mechanisms. can heat up the intra-cluster medium (ICM) as high as $10^8 K$ (Sarazin 2002, 1986). A

medium heated to such an extent is prone to emit X-rays through thermal bremsstrahlung (for a review (Felten et al. 1966; Sarazin 1986), Inverse Compton Scattering of Cosmic Microwave Background Radiation photons by relativistic electrons present in the ICM (Costain et al. 1972; Brecher & Burbidge 1972) and also by thermal synchrotron radiation. So, X-ray luminosity and emissivity for a given photon energy range can be computed from the emission tables created by Smith et al. (2008) with the photoionization code, CLOUDY (Ferland et al. 1998), that includes all the above mentioned emission processes. We have computed the emission fields for photon energy range from 0.1 keV to 12.0 keV , which is the *XMM-Newton* limit and most of the X-ray telescopes are working within this range. This range also includes more than 99% of bolometric luminosity. From our simulations, using the above mentioned relations, we have computed the temperature weighted X-ray emissions.

4.2 Non-thermal cosmic ray emission

In this work, we model the acceleration of CR electrons by injection of available energised particles at the shocks. Injected particle population contains thermally accelerated particles as well as the pre-existing cosmic ray particles due to historical energetic events in the system as discussed in the section 1. These particles further get accelerated by the collision less shocks, mainly via Fermi I process or Diffusive Shock Acceleration (DSA). A fraction of the shock kinetic energy is thus transferred to the CRs. If the acceleration efficiency of the shocks is considered to be $\eta(\mathcal{M})$, the CR energy flux at the shock can be quantified by

$$f_{CR} = \eta(\mathcal{M}) \times f_{kin} \quad (4)$$

where \mathcal{M} is the shock Mach number, f_{kin} is the kinetic energy flux and given by $f_{kin} = \frac{1}{2}\rho v^3$ for a density ρ and velocity dispersion of the medium Kang et al. (2007); Kang & Ryu (2013). Expressing Mach number of the shock as $\mathcal{M} = v/c_s$ with flow velocity v and sound speed in the medium as c_s , kinetic energy flux can be written as a function of shock Mach number \mathcal{M} . The CR flux then becomes a steep function of Mach number only and can be expressed as

$$f_{CR} = \eta(\mathcal{M}) \times \frac{1}{2}\rho(\mathcal{M}c_s)^3 \quad (5)$$

where cosmic ray acceleration fraction i.e. $\eta(\mathcal{M})$ considering pre-existing accelerated particles can be obtained as a fitting function given by Kang et al. (2007).

Cosmic rays produced by a shock can be computed as a function of gas density, shock velocity and radius (Berezinsky et al. 1997). For typical clusters, the roughly estimated value for cosmic ray luminosity from a shocked surface will be almost $10^{43} \text{ erg s}^{-1}$ (Sarazin 2003). This calculation is valid for an ideal case where a single shock has emerged from a major merger of two groups. In the more realistic scenario probed by the numerical simulations, most of the mergers either pass through the phase of core oscillations producing multiple shocks or else multiple mergers take place within a short period of time producing numerous shock surfaces inside the clusters. Also, as only the supersonic shocks contribute to particle acceleration, we have considered only the shock surfaces that contains supersonic shocks. To capture

all these shocks and their contribution to the CR production, we have considered all those shock surfaces and computed the average CR flux over the whole volume of the cluster. Finally, we have computed the CR luminosity for the whole virial volume of the cluster using the relation

$$L_{CR} = 4 \pi V_r^2 f_{CR} \quad (6)$$

Where V_r is the virial radius at over density 200 of each clusters. Since we have captured all the shocks within the virial volume of the clusters in this model, a higher average value i.e. 10^{45} erg s⁻¹ of CR luminosity has been obtained.

5 UNDERSTANDING THE DYNAMICAL STATES OF THE SIMULATED SYSTEMS

5.1 Kinetic and potential energy and the dynamical states of the systems

In this Section we will further elaborate on the difference between merging and non merging clusters, by studying the time evolution of kinetic and potential energy during the cluster history. In Fig. 4 one can see that, during the whole time span and for both representative clusters, the potential energy is larger than the kinetic component. In the upper row of the Fig 4 evolution of different parameters are plotted for a cluster (Cl₅ in our Table 1) that has not seen a prominent merger during the last 8 Gyr of its evolution. Though, the Fig. 4(a) and Fig. 4(b) show, mass and energies of the system have grown almost 3 times during this period, the ratio of energies (i.e. \mathcal{R}_2) has not changed significantly, rather, remained almost constant (Fig. 4(c)). This indicates that a relaxed system, when accreting mass smoothly or through minor mergers, gets enough time to adjust the energy fraction to hold its hydrostatic equilibrium. In the lower row of Fig 4, we have plotted the time evolution of the same quantities for Cl₇, a cluster that has gone through one significant merger during the same evolution time of 8 Gyr. Fig. 4(d) shows a sudden tripling of mass and subsequent slower mass accretion onto the newly formed system which resulted in rapid increment of potential energy within half a Gyr time (in Fig. 4(e)). The growth of the kinetic energy has some time delay with respect to the potential energy. Energy ratio rises very fast, but rate of fall in the energy ratio is much slower and the system takes about 2 Gyr to come back to its pre-merger state (see Fig. 4(f)).

Further, to study the spatial evolution of different energies within a cluster at different dynamical conditions, the radial profile of virial ratio has been plotted (see Fig 5). For this study, our virial ratio definition has been modified slightly than as it is defined in Section 3.1.2. External potential by definition is the potential due to the mass outside virial radius i.e., mass residing between r_{200} to at most the second turn around radius. So, inside the virial radius, the quantity becomes ill defined and show spurious results. Considering this fact, for radial studies, we have modified the virial ratio definition as

$$\mathcal{R}'_1 = \frac{(U_{int} - E_s)}{2 * KE} \quad (7)$$

To make it easier to understand, in Figs. 5(b) and (c) we plot the over-density ratio on the x -axis. Virial radius in

this scale would be plotted as r_{200} . Use of this scale makes it easier as it automatically normalises the x axis for comparing a cluster at different times of its evolution. The radial profiles of this quantity \mathcal{R}'_1 have been plotted in Fig. 5(b) at selected times during the evolution of the cluster Cl₂. Each of these times have been chosen to correspond to specific phases during the merger and subsequent relaxation, as visualised and marked in the evolution of \mathcal{R}_1 (Fig. 5(a)). A merger event in Cl₂ has started at look back time of $t=3.78$ Gyr which is depicted by dashed lines. The next one shows the time at $t=2.84$ Gyr when potential energy gained due to mergers has mostly been converted to kinetic energy i.e. highest kinetic energy phase and shown as dot-dash line. Finally, at 1.54 Gyr, when the cluster has again come to relaxed condition, has been shown as dotted line.

Fig 5(b) shows a possible deviation from the well known spherical accretion model. Core of the clusters in our simulations never seem to remain in virial equilibrium. Though, in relaxed phase, virial ratio \mathcal{R}'_1 makes up to almost 1 at r_{200} , both merging and relaxing phases show a significant deviation from unity. As we go inside the cluster, the merging state is dominated by potential energy, whereas, relaxing state is mostly dominated by kinetic energy (see Fig. 5(c)). But, only in case of relaxed condition, maximum range of x -axis of the cluster till r_{200} has values near to unity.

5.2 Shocking the cluster medium

We have studied the shock properties inside the clusters, mainly the representative parameters of shocks such as shock strength and area that determines the CR emission in the cluster medium. For this study, we have considered the region inside the virial radius (i.e. r_{200}). Within this cluster volume, shocks have been identified with means of unsplit velocity jumps across the cells (Skillman et al. 2008).

In the simulated clusters, in general it is found that the shock Mach numbers are in the range $\mathcal{M} = 1 - 2$ in the core region i.e. r_{1000} . It goes to almost $\mathcal{M} = 4$ in regions beyond the core but inside virial radius (i.e. r_{200}) (Fig. 6 is shown as a representative map). It rarely reaches as high as $\mathcal{M} = 10$. Outside the virial radius (i.e. r_{200}) it goes beyond $\mathcal{M} = 10$. The shocks inside the virial radius are usually called the internal shocks (Miniati et al. 2000; Skillman et al. 2008).

Numerical shocks in grid-based schemes are typically spread over 3 cells in the direction of shock normal. The shocked surface area has been approximated as the sum of the face area of the cells tagged as shocked (See Vazza et al. (2017)). We have further plotted the percentage of area of shocked cell surfaces to the total surface area at r_{200} for the cluster Cl₂ for Mach numbers above 2 and for the last 8 Gyr of its evolution (see the Fig. 7). It is also seen in the merging clusters that most of the shocked cell area is actually occupied by the shocks with Mach number between $\mathcal{M} = 2 - 5$ (dashed line in Fig. 7(a)). This plot clearly reveals that during merger, shocked cell surface area (SCS) occupies more than 200% and reaches as much as 400% in certain most active phases of the total virial surface area of the cluster, with a sharp contrast to the usual shocked cell surface of 100% percent or less in the cluster in relaxed condition (Fig. 7(a), dotted line). Another important observation is that, at the low redshift, the SCS rapidly falls down by about an order of magnitude. In a relaxed system, Mach number beyond

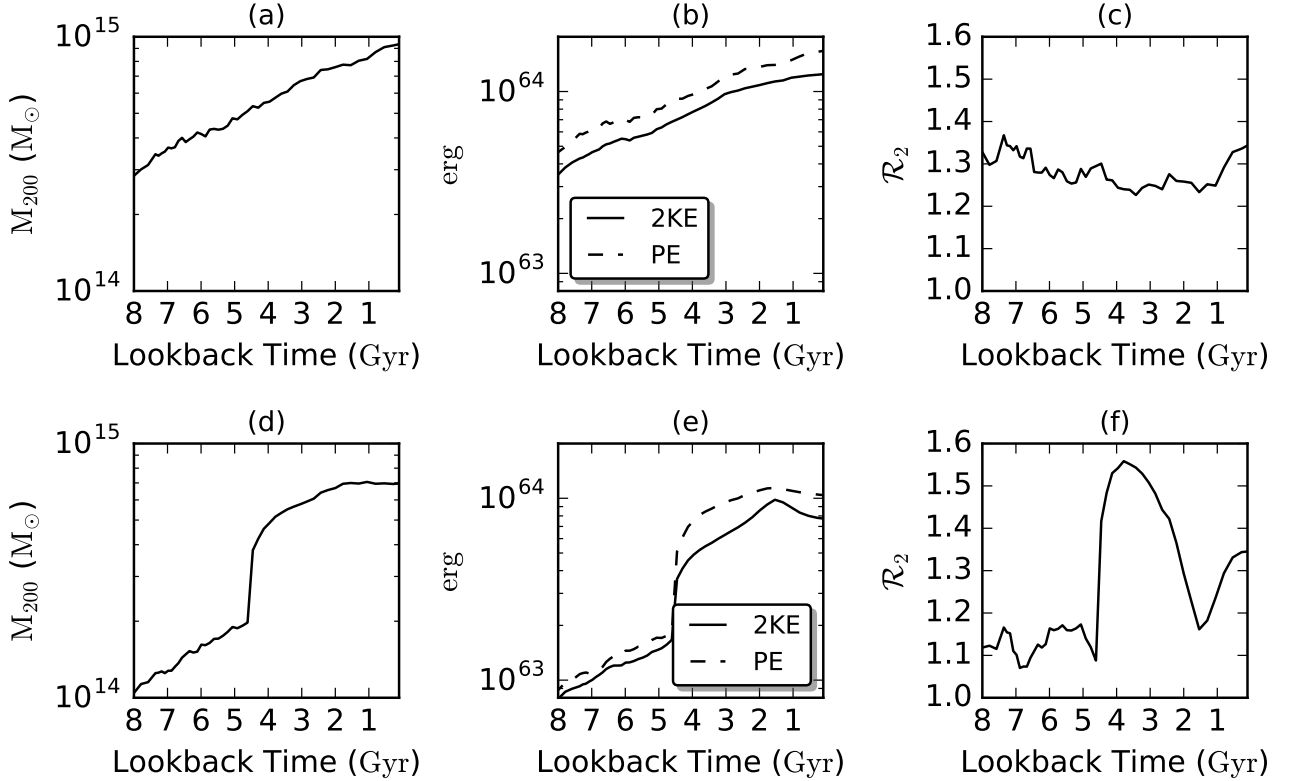


Figure 4. Time evolution of Mass, P.E. and 2K.E. and ratio R_2 (Panel (c)) have been plotted in the three panels (Panel (a), (b) and (c)) respectively for a relaxed Cluster (Cl₅ of Table 1). Same quantities are plotted (in Panel (d), (e) and (f)) for a prominent single merging system (Cl₇ of Table 1).

$\mathcal{M} = 10$ is hardly reached, whereas, during mergers, surface of strong shocked cells sometimes increase by about 10^2 folds than that of a relaxed system (see Fig. 7(b)).

6 DYNAMICAL STATES AND ITS CONNECTION TO ENERGY EVOLUTION

6.1 Energetics of evolving dynamical states of galaxy clusters

In this Section, we will combine both the defined diagnostics for the dynamical state of a cluster and the proxies to observables quantities to get an overall impression on their correlation during the cluster formation history. In our simulations, the main representative merging cluster i.e. Cl₂ has gone through multiple mergers during its 8 Gyr of evolution time as shown using the total mass plot in Figure 8(a). This clearly indicates three major mergers roughly at look-back time of 6, 4.5 and 3 Gyr with merging mass ratio varying in the range of 1:1 to 1:3. Virial ratio R_1 (see Section 3.1.2)

which represents the dynamical state of the system (see Section 3.1.2 and 5.1) peaks at these points indicating a significant change in dynamics of the system (see Fig. 8(b)). On each merger, the total energy (computed as the sum of radial averaged quantity) of the system (thermal energy plus kinetic energy of baryons) increases substantially (see Fig. 8(d)). It is important to stress that the total energy of the system peaks almost a Gyr after each merger as indicated in mass (Fig. 8(a)) and in the virial ratio (Fig. 8(b)). And each instance the time delays of energy are almost the same (i.e. about one Gyr); at about look-back time 5, 3.5 and 2 Gyr respectively (Fig. 8(d)). These are at the same point of time when virial ratio has become lowest after each merger (Fig. 8(b)). The baryon kinetic energy also peaks almost at the same time. This is consistent with theory as these are the phases where most of the potential energy is supposed to be converted to kinetic energy. It is also noticed that relative increment in gas thermal energy is slightly more than the relative increment in total energy. This is due to the gas gaining energy by interaction of baryon particles as well as the additional PdV work by the shocks (Sarazin 2001). The intracluster medium dissipates a fraction of this energy through different radiation processes within less than a Gyr. Through bremsstrahlung X-rays emission, the system loses its thermal energy while the kinetic energy gets used up to produce cosmic rays by shock acceleration of charged particles. Our results (Fig. 8(f)) show that the phase of X-ray luminosity gain coincides with the gas thermal energy gain

¹ Since luminosity has been calculated from all shocked cells emerged inside the cluster virial volume and there can be many shocks (as seen in Fig. 6) filling most part of the volume with multiple layers, we can get more than the surface area of the cluster as shocked.

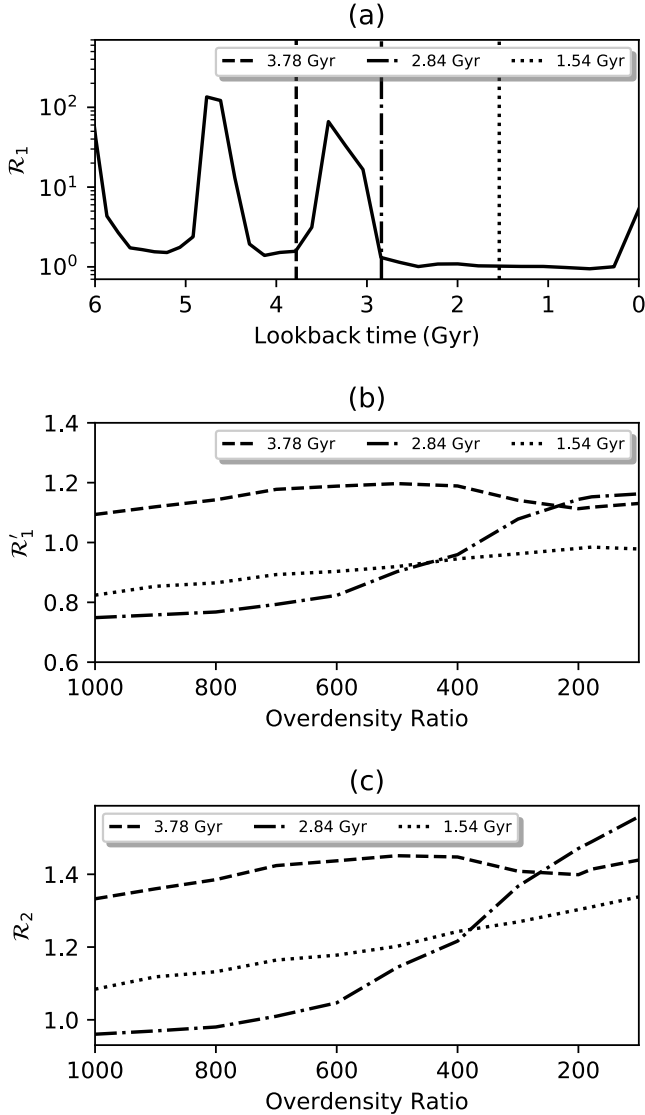


Figure 5. **Panel (a):** Time evolution of virial ratio \mathcal{R}_1 has been plotted for cluster Cl_2 . Specific dynamical states are demarketed on it by dashed line (just after merger), dot-dashed (post merger, KE dominant phase) and dotted line (relaxed phase). **Panel (b):** Shows the radial profile of \mathcal{R}'_1 at the specific phases demarketed in Panel (a). **Panel (c):** Shows the profile of \mathcal{R}_2 against radial overdensity ratios for the same states.

due to mergers. Though the cluster starts emitting X-rays in plenty almost a Gyr year after the mergers, cosmic rays take more than one and half Gyr year to reach the peak (Fig 8(h)). The time delays of X-ray and CR peaks are consistent in all three mergers for Cl_2 as well as in all other merging clusters (Table 1). The brightest phase of CR emission occurs about 1.5 Gyr after the merger has taken place.

Though the total energy of the system due to mergers increases only by few times in magnitude, the CR flux shoots up to almost two orders in magnitude. Here, we have also noticed that the first merger gives out the brightest CR emission peak. In later mergers, CR emission does not gain as much as it had in the first merger (see Fig. 8(h)). The same trend applies also for the X-ray although the to-

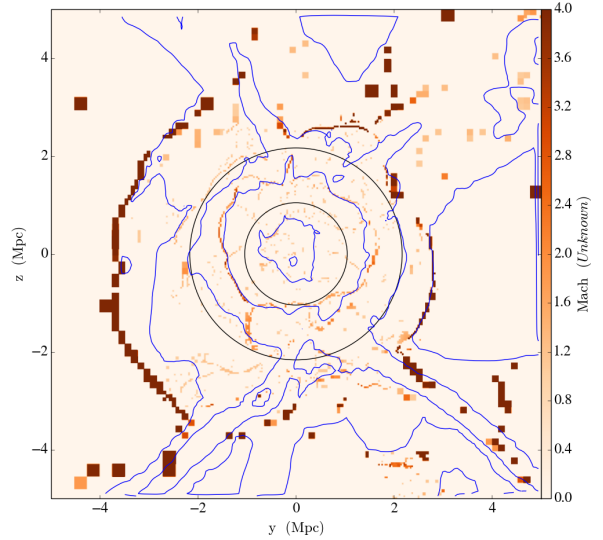


Figure 6. Mach number is plotted in a slice of size of $10 \text{ Mpc } h^{-1}$ each side. Two concentric circles representing radius at overdensity 1000 (r_{1000}) i.e. core and overdensity 200 (r_{200}) i.e. virial radius. Density contours are plotted in blue with highest contour level at $1 \times 10^{-26} \text{ g cm}^{-3}$ to at the lowest at $1 \times 10^{-33} \text{ g cm}^{-3}$.

tal energy of the cluster keeps growing at low redshift. (see Fig. 8(f) and Fig. 8(h)). The outcome is also supported by the fact that at lower redshift shocked cell area consistently decreases (see Fig 7(a)) reducing both shock heating and CR acceleration efficiency. It is also noticed that percentage of fall in total luminosity is more in CRs (see Figure 8, Panel (f),(h)). From the figure 8(e),(g) it can be seen that though merger happens due to rapid accumulation of mass, X-ray and CR emission is not correlated with mass.

6.2 Merging state and its connection to cluster energetics

In Figure 9, we have compared the mass accretion history and the luminosities in X-ray and CR of merging and non-merging systems (see section 3.1.1). Different colours represent different clusters. We have observed that a single significant merger can alter the energy distribution of the system and can dominate for over 2 Gyr (see Fig 4). A major merger can induce turbulence in the system that persists for more than 2 Gyr and up to 4 Gyr in case of core oscillations (Paul et al. 2011) i.e. almost half of its evolution time scale. Cluster mergers are also capable of altering energy budget up to few virial radii from the centre (Iapichino et al. 2017). If this point is considered in terms of cluster scaling laws, it brings to the suggestion that a system once merged may permanently deviate from the scaling that a non-merging system would follow (Ascasibar et al. 2006; Krause et al. 2012). Such deviation happens due to transfer of thermal to non-thermal energy (Yu et al. 2015). Scaling laws in X-rays (thermal) and CRs (non-thermal) would then indicate it.

In Figure 9, the left column shows different parameters of non-merging systems and the right column shows that of merging systems. In Figure 9(a), four non-merging systems have been plotted that show a smooth increment of mass

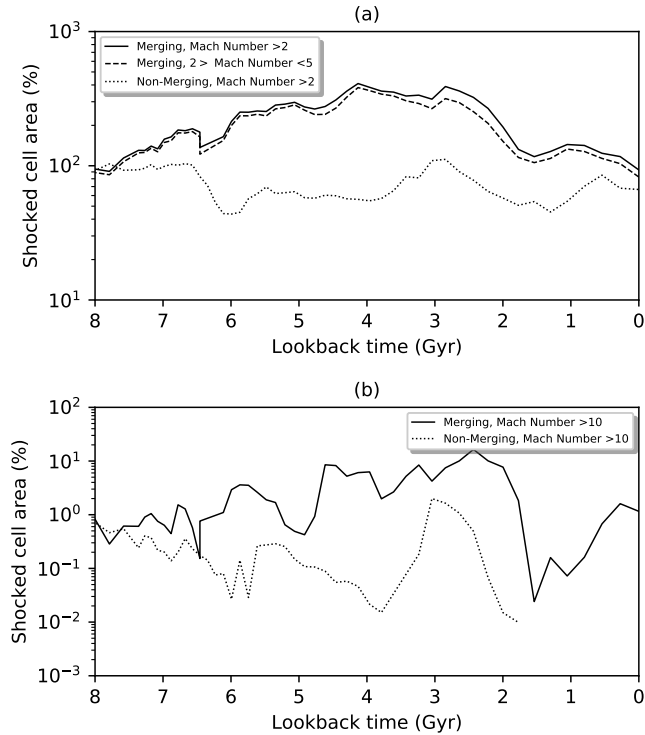


Figure 7. **Panel (a):** shows the time evolution of percentage of shocked cell surface area (of Mach number $\mathcal{M} > 2$ (solid line) and $2 < \mathcal{M} < 5$ (dashed line) for the merging cluster (Cl_2) and $\mathcal{M} > 2$ (dotted line)) for non-merging cluster (Cl_5). The values are normalised to the virial (r_{200}) surface area of the clusters at that point of time. **Panel (b)** Shows the shocked cell area for $M > 10$ for the same merging (solid line) and non-merging (dotted line) systems as above respectively.

for evolution time of 8 Gyr. On the other hand Figure 9(b) shows six merging clusters having one or multiple jumps in total mass, indicating that a merger has occurred in the system. In Figure 9(c) and (d), we have plotted the corresponding CR luminosity. Though the time evolution of mass looks rather smooth outside merger events, so is not for the evolution of L_{CR} . The evolution of this quantity shows numerous fluctuations with time, pointing to the extreme sensitivity of the CR acceleration to even minor variations of the shock location and strength in the ICM. The cosmic ray emission shows a jump of several orders of magnitude each time a cluster goes through a significant merger. This behaviour can be observed for all the merging systems as plotted in panel (d). The finding described in the section 6.1 found stronger support in Figure 6.2(b) and (d), where, it can also be noticed that the major CR emission peaks come approximately after 1.5 Gyr from every significant mass jump i.e. the mergers. While looking at a large number of systems in our sample, we have noticed (in Fig. 9(g) and (h)) that the clusters with same masses, the average CR luminosity of a non-merging system is almost an order of magnitude less than that of a merging system (compare Fig. 9(c) and (d)). From the same figure,

a key conclusion can be drawn about the non-efficient CR acceleration in the high mass systems. It shows that though the initial mergers bring up the CR population to several orders of magnitude higher than its value at relaxed condition, CR population falls to the level of almost same as the non-merging systems in the final stage of its evolution. Possibly, a cluster that goes through earlier mergers is hotter than the usual clusters. This hot medium will reduce the Mach number of the internal shocks and therefore the shocked surface area and as a consequence DSA becomes less effective.

6.2.1 Scaling relations for merging and non-merging systems

In figure 9, Panel (e) to (h), we show the evolution of X-ray and CR luminosity in six merging clusters and four non-merging systems. The points in the plots with same colour represent the same cluster at different times during its evolution. The comparison of the resulting scaling laws $L_{CR} \propto M^\alpha$ and $L_X \propto M^\beta$ show a clear difference between the merging and non-merging systems. While merging systems show a steeper slope $\alpha = 1.68$ for CR luminosity with high scatter value of $\sigma = 0.15$, non-merging systems are following much flatter slope of $\alpha = 1.00$ with lower scatter value of $\sigma = 0.08$. The situation got just reversed in case of X-ray emission where merging clusters have much flatter slope of $\beta = 1.01$ (with $\sigma = 0.06$) than the non-merging one which is $\beta = 1.40$ (with $\sigma = 0.04$). This indicates that merging significantly changes the energetics of the galaxy clusters. This can be an alternative tool to make a distinction between the sets of systems and their dynamics by determination of merging and non-merging states.

6.3 Virialisation and its connection to cluster energetics

In Section 3.1.2 and 5.1, other than the mergers, we have devised another method of determining the dynamical phase of any galaxy cluster using virialisation as the yardstick. Figure 2 and 5 clearly indicate a difference in the dynamics of the clusters according to its state of virialisation. As discussed in the last paragraph of section 3.1.2, we have classified systems as virialised and non-virialised and further the non-virialised systems to HighPE and HighKE. We have already discussed in section 5.1 and 6.1 about how this categorisation helped us in understanding the energy evolution in individual clusters. Further, we will try to use this method for distinguishing objects using the large sample set.

We have noticed that the clusters in merging state gain high potential energy very rapidly. But, significant heating of the medium along with increment in kinetic energy happens in the post-merger phase when the medium tries to attain equilibrium through generation of shocks, a phenomenon called as ‘violent relaxation’ (Wise & Abel 2007). Heating continues till the cluster again comes to relaxed state. This can be understood from the thermal X-ray emission shown in Figure 8(f) and in a large sample in Figure 9(f). Further, cosmic rays, the by product of shock acceleration becomes dominant only after a Gyr from the merger i.e. in the post-merger phase. Since, the central part of the cluster is the

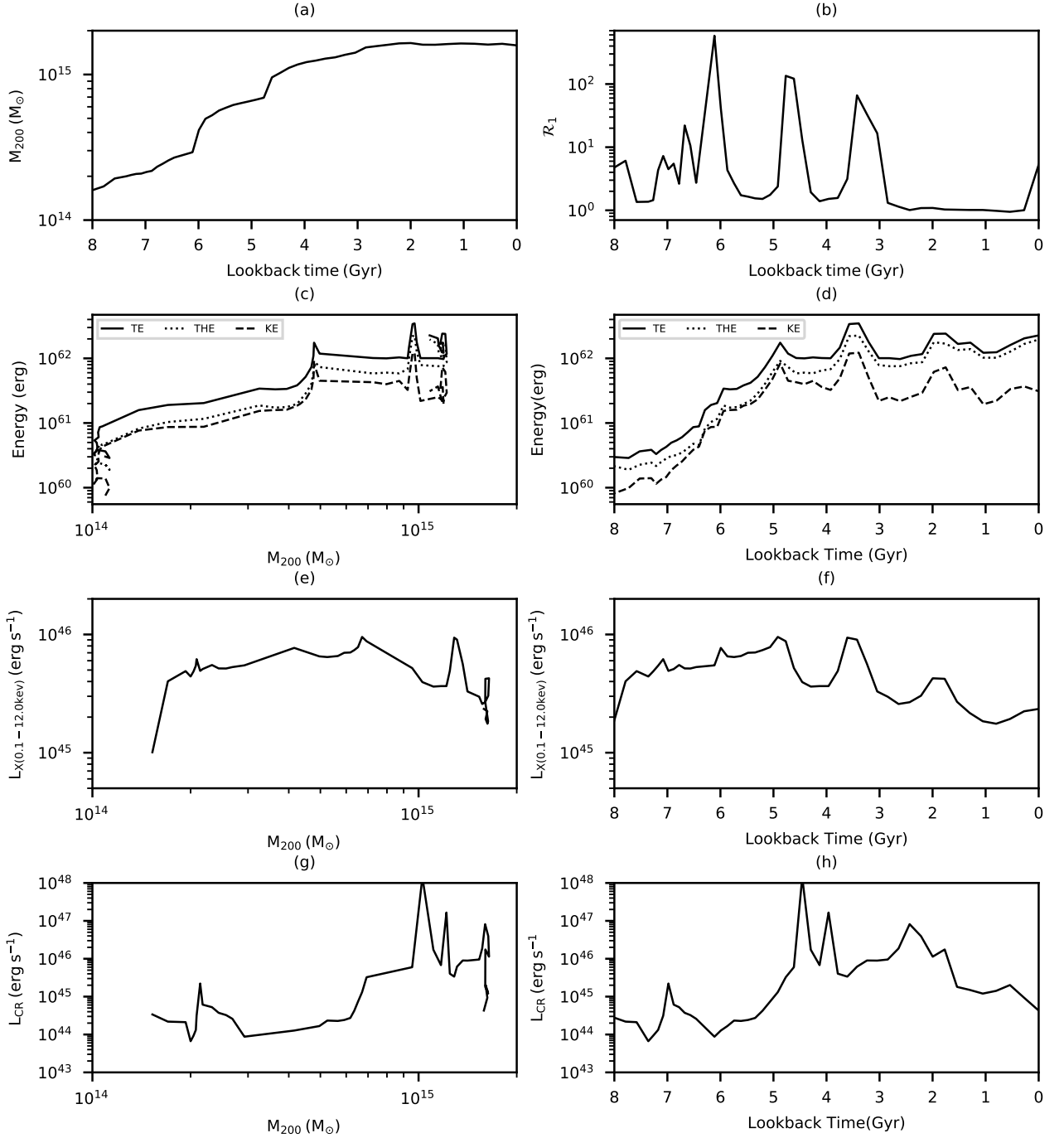


Figure 8. Eight panel plot of our representative merging cluster (Cl₂ of Fig. 3). Mass and R_1 has been plotted with lookback time in Panel (a) and (b) respectively. Total, thermal and kinetic energy have been plotted against M_{200} (c) and Lookback time (d). Further, X-ray luminosity and CR luminosity evolution shown against M_{200} (Panel (e) and (g) and lookback time (Panel (f) and (h)).

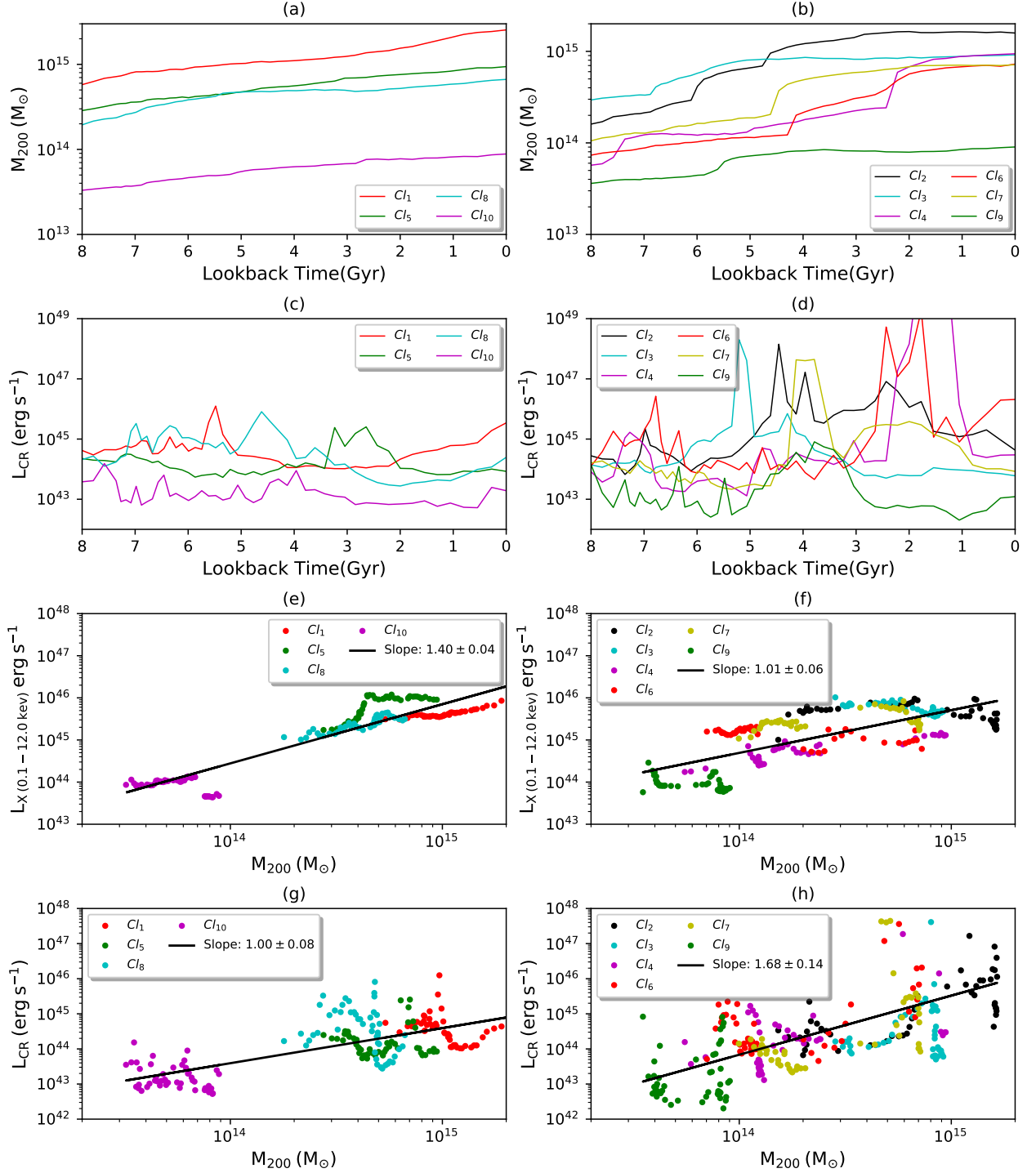


Figure 9. Evolution of mass and CR flux has been plotted against lookback time in Panel (a)&(c) and X-ray luminosity and CR luminosity has been plotted against virial mass of the non-merging clusters in the Panel (e)&(g). The same parameters has been shown for merging clusters in Panel (b),(d),(f) and (h) respectively

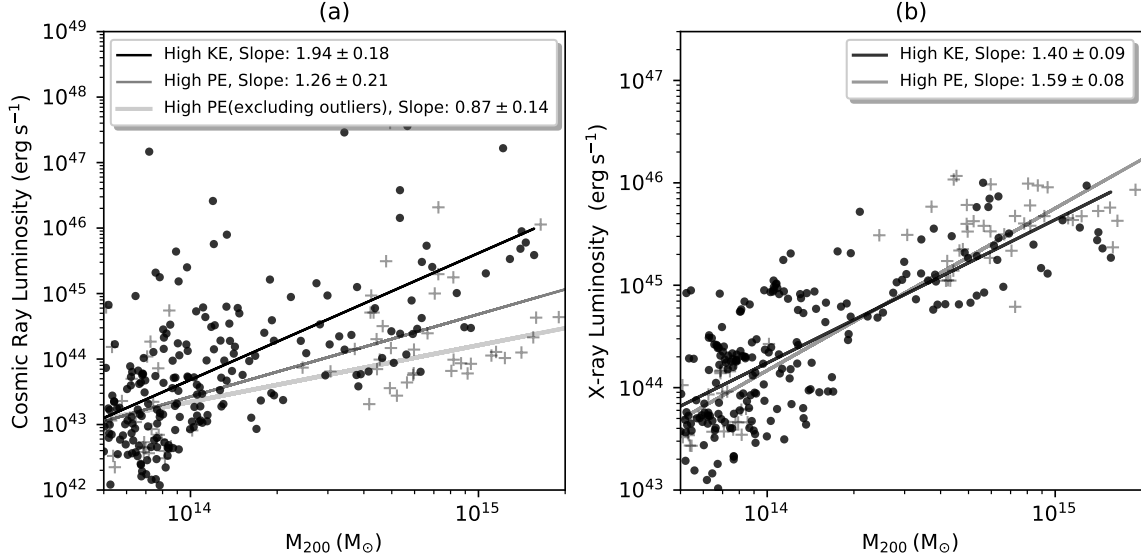


Figure 10. CR (Panel (a)) and X-ray luminosity (Panel (b)) of HighKE (dark dots) and HighPE (grey plus) has been plotted against the mass (M_{200}).

hottest, Mach number of the shock is usually low there i.e. below $\mathcal{M} = 2$ (within r_{1000}). Shock becomes stronger beyond the cluster core where the medium is relatively colder. Most of the shocks with Mach number $\mathcal{M} = 2 - 5$ are found between r_{1000} and the virial radius (i.e. r_{200}) of the cluster (see Fig 6). This tells us that the thermalisation and particle acceleration actually takes place only in the post-merger phase (i.e. HighKE) indicating the introduction of a significant change in energy distribution in the ICM at post-merger compared to the virialised and merger phase (i.e. HighPE).

6.3.1 Scaling relations from the state of virialisation

Since dynamical activity in the galaxy clusters modifies the energy budget of the clusters, the contribution to luminosity from the thermal and non-thermal components are expected to change during the cluster evolution. In Fig 10, we have plotted X-ray and CR luminosity of HighKE and HighPE. Figure 10(a) shows that cluster with highKE has significantly gained cosmic ray emission with very steep mass spectrum i.e. slope 1.94, with $\sigma = 0.18$. The scaling exponent of the HighPE clusters is much flatter 1.26 ± 0.21 . We notice that the slope of HighPE objects are almost similar to the virialised objects (1.28 with $\sigma = 0.16$). When we further removed few outliers ($> 10^{45} \text{ erg s}^{-1}$) from the HighPE data set, slope became much flatter (0.87 ± 0.14). X-ray emission from HighKE (slope 1.40 ± 0.09) does not show much difference with the HighPE objects (slope 1.59 ± 0.08), but the marginal change of the scaling slope is in the opposite direction to CRs which is in well agreement with the finding in section 6.2.1. Importantly, it can also be noticed from these slopes that the average CR energy is about 10 – 15% of the X-ray energy in all mass ranges for HighPE objects (see Figure 10(a) and (b)). But, for objects at the high mass ($M \geq 5 \times 10^{14} M_{\odot}$), the candidates of HighKE group have a larger L_{CR} value than the one of the HighPE group. The dif-

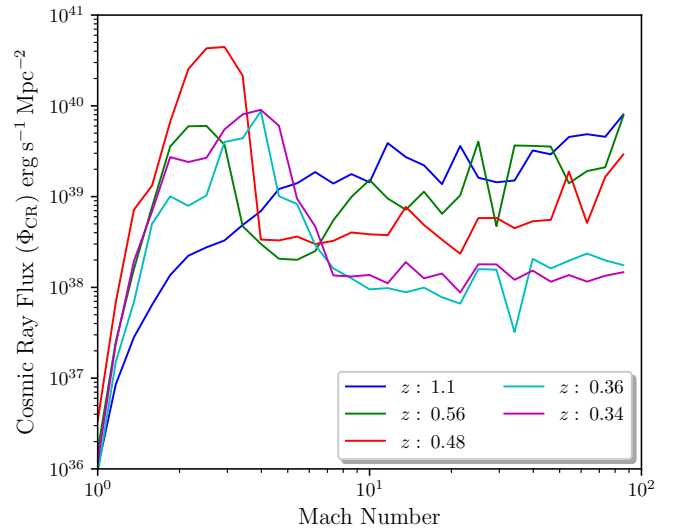


Figure 11. Cosmic ray flux has been plotted against Mach number at different redshifts for the cluster Cl₂

ference is up to an order of magnitude, and HighKE clusters have L_{CR} as large as their L_X . This becomes an indicator of post-merger and non-virialised systems for the high mass objects.

6.4 Mach number distribution and its connection to CR emissions

Cosmic ray emissions due to particle acceleration is usually known to be a steep function of shock strength (Ryu et al. 2003). In Figure 11, the evolution of the CR flux as

a function of the shock Mach number for the representative merging cluster Cl_2 is shown. The plot clearly shows that the most CR acceleration is happening for the Mach number ranging $\mathcal{M} = 2 - 5$ (peak at about $\mathcal{M} = 3$) during the evolution of the merging clusters is in agreement with the work of [Hong et al. \(2014\)](#). We have also found that the peak of cosmic ray emission is seen to move towards higher number starting from $\mathcal{M} = 2.5 - 3.5$ as the time passes after a merger. This happens on a time scale of $2 - 3$ Gyr during each mergers. Similar plots as Figure 11 for other merging clusters, not shown here, demonstrate that the range and the peak slightly varies in different merging clusters in our sample but the basic trend holds for all mergers. This also indicates that most of the CR acceleration is probably happening due to the main merger shock (see Section 5.2), which increases its Mach number while propagating in a colder medium towards the cluster outskirts.

We further notice that this variation of range and the peak of effective Mach number is a steep function of the shock area. Figure 7(a) shows the differential area with Mach number ranges. It is evident from this plot that almost all shocked cells are associated to shocks with Mach number in the range $\mathcal{M} = 2 - 5$, while, Mach number above $\mathcal{M} = 10$ is occupying very minor fraction of the virial surface area (about 10% only, see Fig. 7(b)). Shocked area in Cl_1 , the non-merging cluster, is seen to be almost flat and stays at a level of 100% or below throughout the cluster evolution. The same behaviour is also shown by the CR luminosity which has a rather flat evolution with time and stays at a level of $10^{44-45} \text{ ergs}^{-1}$ (Fig. 9(c)). It has also been noticed that at low redshift, the shocked area in the merging cluster Cl_2 has decreased to a value typical of non-merging clusters. As a consequence, also its CR luminosity decreases to a value typical of non-merging objects $10^{44-45} \text{ ergs}^{-1}$, Fig 9(d).

7 LIMITATIONS OF THIS STUDY

Since DSA is widely accepted to be the main mechanism behind cosmic ray acceleration in the large scale structures ([Kang et al. 1997](#); [Miniati et al. 2001](#)), our study considers only DSA as the particle acceleration mechanism. In this context, some researcher has also pointed out about the contribution from turbulent re-acceleration ([Brunetti 2016](#); [Brunetti & Lazarian 2011](#); [Eckert et al. 2017](#)). We are well aware of the important role of AGN activity and SN explosion in the CR acceleration, especially for providing a pristine CR pool for both DSA and re-acceleration model ([Kang et al. 2007](#); [Brunetti & Lazarian 2011](#)). Though our model of CR acceleration by DSA considers pre-existing CR population ([Kang et al. 2007](#)), turbulent re-acceleration or their (AGN and SN) direct contribution has not been included here. Further, our computation of CR acceleration is done using the fitting model of [Kang et al. \(2007\)](#) as the post process of parameters obtained from the snapshots taken from our hydrodynamics plus N-body simulations. So, this calculation considers only instantaneous CR acceleration, and no time evolution solutions. However, the peak of CR luminosity for merging clusters is in some cases one order of magnitude or more larger than the pre-merger value, partly justifying the instantaneous approach for the CR acceleration in those cases. CR transport mechanism has also been ignored

here. Since, the physical process of CR emission evolves with time and transport of high energy particles alters its energy and distribution, to obtain a more realistic picture one has to implement all the above mentioned physics in the calculations.

8 SUMMARY

In this paper, we are reporting an extensive study on the origin and temporal and spatial evolution of cosmic rays in merging and non-merging galaxy clusters. We have performed cosmological simulations with the Enzo AMR code ([Bryan et al. 2014](#)). In this study, the origin and evolution (in time and space) of cosmic rays in merging and non-merging clusters is elucidated in detail for the first time (see Section 6.2). We find a strong connection between the dynamical states of galaxy clusters and the emission of CRs. Energy distribution in clusters are shown to be directly related to merger activity, fractional area covered by shocks and on how far a cluster is away from virialisation (according to the definition of virialisation in section 3.1.2). The novel method of quantifying virialisation and the different scaling laws on dynamic state of the clusters discussed in this paper serves as a very useful tool for the accurate determination of the phase of merger of any galaxy cluster from a set of observables. The important outcomes of this study are

- Shocks are the most important parameter for CR emissions through DSA. We show that the percentage of shocked surface area in a cluster is crucial for CR emission efficiency. In most of the clusters, Mach number in the range between $\mathcal{M} = 2 - 5$ captures the most of the shocked area and is therefore the most effective generator of CRs. Since this is the Mach number range of internal or merger shocks, it can be inferred that merger events are the most efficient engines for CR acceleration from clusters, rather than the high Mach number accretion shocks.

- Our study shows that there is a consistent time delay in the peak luminosities of X-ray and CR, considered to be the tracers of thermal and non-thermal energy production during merger events. The X-ray luminosity and total energy of merging galaxy clusters are observed to attain a maximum after 1 Gyr of the merging event, whereas, CR luminosity reaches its peak after 1.5 Gyr after the merger. So, the expectations of concurrence of events in morphology, thermal energy and the non-thermal energy ([Reimer et al. 2003](#); [Huber et al. 2013](#); [Schönfelder 2001](#)) is proved to be not holding good. This is suggested to be the reason for many of the X-ray bright clusters did not show up in Gamma rays, radio as well as in other non-thermal emissions.

- Clusters with merging history permanently deviates from the mass scaling laws with X-ray and CR luminosity of non-merging systems (see Section 6.2.1 and Figure 9, Panel (e) to (h)). For non-merging clusters, it is observed that slope is flatter for CRs (i.e. $L_{CR} \propto M^{1.0 \pm 0.06}$) but steeper in X-rays ($L_X \propto M^{1.4 \pm 0.04}$). The contrary can be seen in case of merging clusters where, CR luminosity increases very steeply with mass ($L_{CR} \propto M^{1.7 \pm 0.15}$),

while X-ray luminosity scales linearly ($L_X \propto M^{1.0 \pm 0.08}$). Interestingly, it is observed in the time evolution study in Fig 8 that the mass of clusters is not correlated to luminosity during the mass accretion history, especially as far as L_{CR} is concerned.

- Virial ratio as defined in Section 3.1.2 has been found to be a very useful tool for determining the dynamical state of galaxy clusters. From an observational viewpoint, it is sufficient to get the information on velocity dispersion of the constituent galaxies in a cluster, mass of the system, its size, namely the virial radius and second turn over radius to compute its state of virialisation. This quantity exhibits a distinct peak at the time of merger (see Fig. 1 and Fig.8) enabling it to be used as a tool to determine the actual dynamical state.

- Simulated merging clusters in our sample do not show virialisation inside the overdensity ratio of r_{200} (see Fig. 5). During the merger phase, the core is dominated by the potential energy, whereas, during the violent relaxation phase, it is mostly dominated by the kinetic energy. The similar finding has been reported in Shaw et al. (2006). The apparent discrepancy with the simplified case of the spherical collapse model can be attributed to the complexity of cosmological setup with the presence of filaments and numerous sub-structures and their merger activities.

- To better study the properties of non-virialised objects, we divided them into two categories, HighKE and HighPE (see Section 3.1.2 last paragraph for the definitions) the cosmic ray production grows non linearly with mass for HighKE objects ($L_{CR} \propto M^{1.93 \pm 0.18}$) compared to HighPE or virialised objects ($L_{CR} \propto M^{1.26 \pm 0.16}$ and $L_{CR} \propto M^{0.87 \pm 0.14}$ with removed outliers). Conversely, the mass scaling of L_X does not show any substantial difference between the two groups. Hence, high mass clusters with HighKE have L_{CR} at the level of L_X , while HighPE massive clusters (the same argument holds also for virialised clusters) have L_{CR} smaller by one order of magnitude. (see Section 6.3.1 and Figure 10). Because of such behaviour, the cluster CR luminosity can become an indicator of activity for high mass clusters ($> 5 \times 10^{14} \odot$) and can be used as a tool to understand the state of virialisation from the information about X-ray and gamma-ray luminosity of a set of clusters.

ACKNOWLEDGEMENTS

This project is funded by DST-SERB, Govt. of India, under the Fast Track scheme for young scientists, Grant No. SR/FTP/PS-118/2011. We are thankful to The Inter-University Centre for Astronomy and Astrophysics (IUCAA) for providing the HPC facility. Computations described in this work were performed using the Enzo code developed by the Laboratory for Computational Astrophysics at the University of California in San Diego (<http://lca.ucsd.edu>) and data analysis is done with the yt-tools (<http://yt-project.org/>).

REFERENCES

- Ackermann M., Ajello M., Albert A., Atwood W. B., Baldini L., Ballet J., Barbiellini G., Bastieri D., Bechtol K., Bellazzini R., Fermi-LAT Collaboration Rephaeli Y., 2016, *ApJ*, 819, 149
- Aguerre J. A. L., Sánchez-Janssen R., 2010, *A&A*, 521, A28
- Akahi T., Yoshikawa K., 2012, *PAJS*, 64, 12
- Arnaud M., Pointecouteau E., Pratt G. W., 2005, *A&A*, 441, 893
- Ascasibar Y., Sevilla R., Yepes G., Müller V., Gottlöber S., 2006, *MNRAS*, 371, 193
- Bagchi J., Durret F., Neto G. B. L., Paul S., 2006, *Science*, 314, 791
- Bagchi J., Sirothia S. K., Werner N., Pandge M. B., Kantharia N. G., Ishwara-Chandra C. H., Gopal-Krishna Paul S., Joshi S., 2011, *ApJ*, 736, L8
- Ballesteros-Paredes J., 2006, *MNRAS*, 372, 443
- Barsanti S., Girardi M., Biviano A., Borgani S., Annunziatella M., Nonino M., 2016, *A&A*, 595, A73
- Berezinsky V. S., Blasi P., Ptuskin V. S., 1997, *ApJ*, 487, 529
- Berrington R. C., Dermer C. D., 2003, *ApJ*, 594, 709
- Bharadwaj V., Reiprich T. H., Lovisari L., Eckmiller H. J., 2015, *A&A*, 573, A75
- Blandford R., Eichler D., 1987, *Phys. Rev.*, 154, 1
- Blasi P., 2004, *Journal of Korean Astronomical Society*, 37, 483
- Bourdin H., Mazzotta P., Markevitch M., Giacintucci S., Brunetti G., 2013, *ApJ*, 764, 82
- Brecher K., Burbidge G. R., 1972, *ApJ*, 174, 253
- Brunetti G., 2016, *Plasma Physics and Controlled Fusion*, 58, 014011
- Brunetti G., Jones T. W., 2014, *International Journal of Modern Physics D*, 23, 30007
- Brunetti G., Lazarian A., 2011, *MNRAS*, 410, 127
- Brunetti G., Zimmer S., Zandanel F., 2017, *MNRAS*, 472, 1506
- Bryan G. L., Norman M. L., O'Shea B. W., Abel T., Wise J. H., Turk M. J., Reynolds D. R., Enzo Collaboration 2014, *ApJS*, 211, 19
- Bykov A. M., Churazov E. M., Ferrari C., Forman W. R., Kaastra J. S., Klein U., Markevitch M., de Plaa J., 2015, *SSRv*, 188, 141
- Cen R., Ostriker J. P., 1992, *ApJL*, 399, L113
- Choi Y.-Y., Reynolds C. S., Heinz S., Rosenberg J. L., Perlman E. S., Yang J., 2004, *ApJ*, 606, 185
- Costain C. H., Bridle A. H., Feldman P. A., 1972, *ApJ*, 175, L15
- Davis A. J., D'Aloisio A., Natarajan P., 2011, *MNRAS*, 416, 242
- Diaferio A., Ramella M., Geller M. J., Ferrari A., 1993, *AJ*, 105, 2035
- Dolag K., Vazza F., Brunetti G., Tormen G., 2005, *MNRAS*, 364, 753
- Eckert D., Gaspari M., Vazza F., Gastaldello F., Tramacere A., Zimmer S., Etti S., Paltani S., 2017, *ApJ*, 843, L29
- Eisenstein D. J., Hu W., 1999, *ApJ*, 511, 5
- Ellison D. C., Ramaty R., 1985, *ApJ*, 298, 400
- Felten J. E., Gould R. J., Stein W. A., Woolf N. J., 1966, *ApJ*, 146, 955
- Ferland G. J., Korista K. T., Verner D. A., Ferguson J. W., Kingdon J. B., Verner E. M., 1998, *PASP*, 110, 761
- Finoguenov A., Reiprich T. H., Böhringer H., 2001, *A&A*, 368, 749
- Hong S. E., Ryu D., Kang H., Cen R., 2014, *APJ*, 785, 133
- Huber B., Tchernin C., Eckert D., Farnier C., Manalaysay A., Straumann U., Walter R., 2013, *A&A*, 560, A64
- Iapichino L., Federrath C., Klessen R. S., 2017, *MNRAS*, 469, 3641
- Iapichino L., Maier A., Schmidt W., Niemeyer J., 2010, in *AIP Conference Proceedings Vol. 1241, Turbulence modeling and the physics of the intra-cluster medium*. pp 928–934
- Jones T. W., Miniati F., Ryu D., Kang H., 2001, in *Aharonian F. A., Völk H. J., eds, American Institute of Physics Confer-*

- ence Series Vol. 558 of AIP Conference Proceedings, Winds and shocks in galaxy clusters: Shock acceleration on an intergalactic scale. pp 436–447
- Kaastra J. S., Bykov A. M., Schindler S., Bleeker J. A. M., Borgani S., Diaferio A., Dolag K., Durret F., Nevalainen J., Ohashi T., Paerels F. B. S., Petrosian V., Rephaeli Y., Richter P., Schaye J., Werner N., 2008, SSR, 134, 1
- Kaiser N., 1986, MNRAS, 222, 323
- Kang H., Jones T. W., 2007, Astroparticle Physics, 28, 232
- Kang H., Rachen J. P., Biermann P. L., 1997, MNRAS, 286, 257
- Kang H., Ryu D., 2013, ApJ, 764, 95
- Kang H., Ryu D., Cen R., Ostriker J. P., 2007, ApJ, 669, 729
- Kang H., Ryu D., Jones T. W., 1996, ApJ, 456, 422
- Komatsu E., Dunkley J., Nolte M. R., Bennett C. L., Gold B., Hinshaw G., Jarosik N., Larson D., Limon M., Page L., Spergel D. N., Halpern M., Hill R. S., Kogut A., Meyer S. S., Tucker G. S., Weiland J. L., Wollack E., Wright E. L., 2009, ApJS, 180, 330
- Krause E., Pierpaoli E., Dolag K., Borgani S., 2012, MNRAS, 419, 1766
- Kushnir D., Waxman E., 2009, J. Cosmology Astropart. Phys., 8, 002
- Kushnir D., Waxman E., 2010, J. Cosmology Astropart. Phys., 2, 025
- Le Brun A. M. C., McCarthy I. G., Schaye J., Ponman T. J., 2014, MNRAS, 441, 1270
- Malkov M. A., 1998, PhRvE, 58, 4911
- Malkov M. A., O’C Drury L., 2001, Reports on Progress in Physics, 64, 429
- Maughan B. J., Giles P. A., Randall S. W., Jones C., Forman W. R., 2012, MNRAS, 421, 1583
- McCarthy I. G., Schaye J., Ponman T. J., Bower R. G., Booth C. M., Dalla Vecchia C., Crain R. A., Springel V., Theuns T., Wiersma R. P. C., 2010, MNRAS, 406, 822
- Miniati F., 2000, PhD thesis, University of Minnesota, USA
- Miniati F., Ryu D., Kang H., Jones T. W., 2001, ApJ, 559, 59
- Miniati F., Ryu D., Kang H., Jones T. W., Cen R., Ostriker J. P., 2000, ApJ, 542, 608
- Nevalainen J., Markevitch M., Forman W., 2000, ApJ, 532, 694
- Nevalainen J., Oosterbroek T., Bonamente M., Colafrancesco S., 2004, ApJ, 608, 166
- O’Shea B. W., Bryan G., Bordner J., Norman M. L., Abel T., Harkness R., Kritsuk A., 2005, in Adaptive Mesh Refinement – Theory and Applications. Springer, Berlin, New York Vol. 41 of Plewa T., Linde T., Weirs V.G, eds, Lecture Notes in Computational Science and Engineering, Introducing Enzo, an AMR Cosmology Application. p. 341
- Paul S., 2012, in Pal S., Basu B., eds, International Conference on Modern Perspectives of Cosmology and Gravitation (COSGRAV12), Journal of Physics: Conference Series, Volume 405 Vol. 405 of Journal of Physics: Conference Series, Cluster merger blast wave and the mystery of ringlike radio-relic formation around some galaxy clusters. p. 012026
- Paul S., Gupta P., John R. S., Punjabi V., 2015, in The Many Facets of Extragalactic Radio Surveys: Towards New Scientific Challenges Uniqueness of galaxy groups in the structural hierarchy from its radio signature. p. 65
- Paul S., Iapichino L., Miniati F., Bagchi J., Mannheim K., 2011, ApJ, 726, 17
- Paul S., John R. S., Gupta P., Kumar H., 2017, MNRAS, 471, 2
- Peebles P. J. E., 1980, The large-scale structure of the universe Petrosian V., Bykov A. M., 2008, SSRv, 134, 207
- Planck Collaboration Ade P. A. R., Aghanim N., Arnaud M., Ashdown M., Atrio-Barandela F., Aumont J., Baccigalupi C., Balbi A., Banday A. J., et al. 2013, A&A, 550, A134
- Ponman T. J., Cannon D. B., Navarro J. F., 1999, Nature, 397, 135
- Reimer O., Pohl M., Sreekumar P., Mattox J. R., 2003, ApJ, 588, 155
- Roettiger K., Burns J. O., Stone J. M., 1999, ApJ, 518, 603
- Ryu D., Kang H., Hallman E., Jones T. W., 2003, ApJ, 593, 599
- Sarazin C. L., 1986, Reviews of Modern Physics, 58, 1
- Sarazin C. L., 2001, in Neumann D. M., Tran J. T. V., eds, Clusters of Galaxies and the High Redshift Universe Observed in X-rays Merger shocks and nonthermal processes in clusters of galaxies *
- Sarazin C. L., 2002, in Feretti L., Gioia I. M., Giovannini G., eds, Merging Processes in Galaxy Clusters Vol. 272 of Astrophysics and Space Science Library, The Physics of Cluster Mergers. pp 1–38
- Sarazin C. L., 2003, Physics of Plasmas, 10, 1992
- Sarazin C. L., White III R. E., 1987, ApJ, 320, 32
- Schönfelder V., 2001, The Universe in Gamma Rays
- Shaw L. D., Weller J., Ostriker J. P., Bode P., 2006, ApJ, 646, 815
- Shimizu M., Kitayama T., Sasaki S., Suto Y., 2003, ApJ, 590, 197
- Skillman S. W., O’Shea B. W., Hallman E. J., Burns J. O., Norman M. L., 2008, ApJ, 689, 1063
- Smith B., Sigurdsson S., Abel T., 2008, MNRAS, 385, 1443
- Springel V., Frenk C. S., White S. D. M., 2006, Nature, 440, 1137
- Turk M. J., Smith B. D., Oishi J. S., Skory S., Skillman S. W., Abel T., Norman M. L., 2011, ApJS, 192, 9
- van Weeren R. J., Brüggen M., Röttgering H. J. A., Hoeft M., 2011, MNRAS, 418, 230
- Vazza F., Dolag K., Ryu D., Brunetti G., Gheller C., Kang H., Pfrommer C., 2011, MNRAS, 418, 960
- Vazza F., Jones T. W., Brüggen M., Brunetti G., Gheller C., Porter D., Ryu D., 2017, MNRAS, 464, 210
- Vikhlinin A., Forman W., Jones C., 1999, ApJ, 525, 47
- Völk H. J., Aharonian F. A., Breitschwerdt D., 1996, SSRv, 75, 279
- Wen Z. L., Han J. L., 2013, MNRAS, 436, 275
- Wise J. H., Abel T., 2007, ApJ, 665, 899
- Xi S.-Q., Wang X.-Y., Liang Y.-F., Peng F.-K., Yang R.-Z., Liu R.-Y., 2017, ArXiv e-prints:1709.08319
- Yu L., Nelson K., Nagai D., 2015, ApJ, 807, 12

APPENDIX A: RESOLUTION STUDY

We show here some resolution studies to test the convergence of our results. The main runs that are used for this study are performed with the cosmological and simulation parameters described in section 3 with 6 levels of total (uni-grid + AMR) refinement leading to a resolution of about 30 kpc. Keeping all other parameters same, we have further simulated some of our objects with different AMR levels to achieve different levels of resolutions. We have produced a lower resolution (‘LOWRES’ hereafter, resolution is about 60 kpc) and a higher resolution (‘HighRES’ hereafter, resolution is about 15 kpc) simulations. Further, to test the convergence of our results, we have performed other two sets of simulations with two different root grids besides the ‘RefRES’. The one with high resolution root grid i.e. 128^3 is named as ‘RootHIRES’ and one with 32^3 root grid as ‘RootLOWRES’. In these test runs, the AMR setup is so chosen that the effective spatial resolution is same as that in reference runs. Finally, we have compared the physical parameters obtained from these simulations.

In Figure A1 radial variations of CR luminosity has been plotted for the clusters Cl_2 (merging) and Cl_5 (nonmerging) in different runs. It can be noticed that the results for the REFRES simulation are almost the same as for

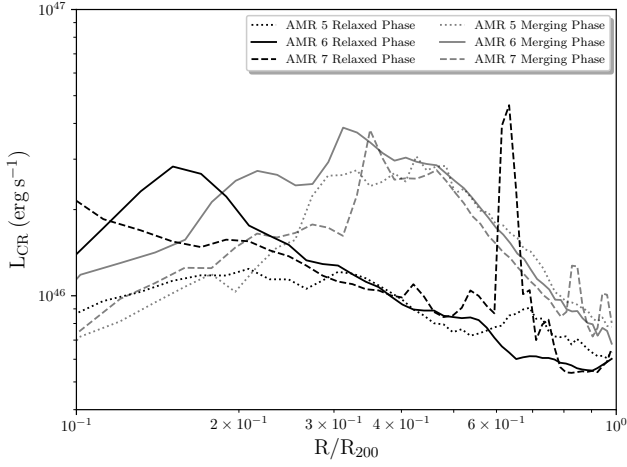


Figure A1. Computed cosmic ray luminosity have been plotted against normalised radius (normalised to r_{200}) for merging and relaxed states (see Fig 4), of a galaxy cluster (Cl_2 , mass about $10^{15} M_{\odot}$) and for three resolutions namely LOWRES, REFRES and HIGHRES (as indicated in the legend respectively).

the HIGHRES run with minor deviation, though, LOWRES data are little away. The peak of the cosmic ray flux can be noticed at cluster centre (for relaxed state) and at the outskirts (for merging phase) as in relaxed state CR population will be dominated by central density and small shocks whereas at merging state when high Mach number shocks reaches cluster outskirts, most CR acceleration will happen there. Small spatial variation that can be noticed among the different resolution plots occurs due to resolution sensitivity of transient phenomena like shocks. It can also be noticed that the merging phases have better convergent results. These results show that our simulated quantities have good convergence with the resolution taken as the reference set of simulations i.e. about 30 kpc with 6 levels of refinement. For further details of resolution study of our data sets, we refer the reader to [Paul et al. \(2017\)](#).

As we have already mentioned above, other two tests with different root grid resolution namely RootLOWRES and RootHiGHRES have been performed. We have then chosen appropriate merging and non-merging states and plotted the CR luminosity at those states. The tests with different root grid resolution is shown in Figure A2. A reasonable convergence in CR luminosity can be observed.

This paper has been typeset from a \LaTeX file prepared by the author.

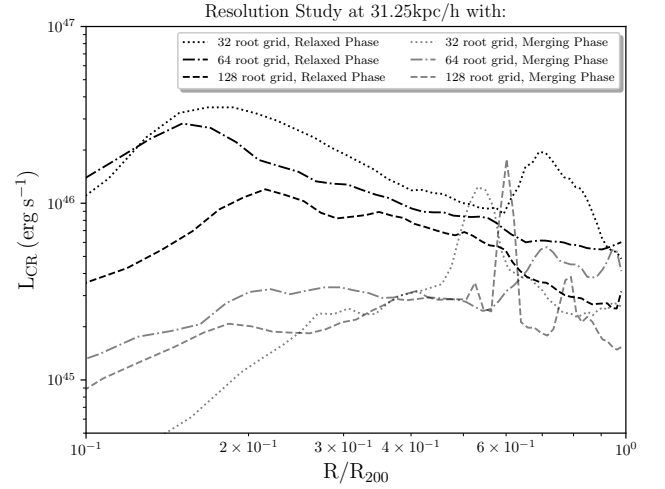


Figure A2. Plot of same phases as in Figure A1 for different root grid resolution simulations with the same final resolution of about 30 kpc.